



Crystal structure of cytochrome P450 CYP105N1 from *Streptomyces coelicolor*, an oxidase in the coelibactin siderophore biosynthetic pathway

Young-Ran Lim^{a,1}, Myoung-Ki Hong^{b,1}, Jin-Kwang Kim^b, Thanh Thi Ngoc Doan^b, Dong-Hyun Kim^c, Chul-Ho Yun^c, Young-Jin Chun^d, Lin-Woo Kang^{a,*}, Donghak Kim^{a,*}

^a Department of Biological Sciences, Konkuk University, Seoul, Republic of Korea

^b Department of Advanced Technology Fusion, Konkuk University, Republic of Korea

^c School of Biological Sciences and Technology, Chonnam National University, Gwangju, Republic of Korea

^d College of Pharmacy, Chung-Ang University, Seoul, Republic of Korea

ARTICLE INFO

Article history:

Received 5 July 2012

and in revised form 30 August 2012

Available online 18 September 2012

Keywords:

P450

CYP105N1

Streptomyces coelicolor

Coelibactin

Estradiol

ABSTRACT

The genome sequence of *Streptomyces coelicolor* contains 18 cytochrome P450 enzymes. The recombinant CYP105N1 protein has been expressed in *Escherichia coli* and purified, and we report the biochemical and structural characterization of CYP105N1 from *S. coelicolor*. The purified protein exhibited the typical CO-binding spectrum of P450 enzymes and type I binding spectra with estradiol and a coelibactin analog. The oxidation of estradiol by CYP105N1, supported by H₂O₂, produced estriol. The crystal structure of CYP105N1 was determined at 2.9 Å resolution. An unexpected wide open binding pocket located above the heme group was identified, with a volume of approximately 4299 Å³. These results suggest that the large open pocket to the active site may be a key feature for easy access of the peptidyl carrier protein-bound substrate to perform the hydroxylation reaction. A molecular docking model with coelibactin showed that the phenyl group of coelibactin is located <4 Å away from the heme-iron, suggesting that CYP105N1 may be involved in the hydroxylation of the phenyl ring of the coelibactin precursor during biosynthesis.

© 2012 Elsevier Inc. All rights reserved.

1. Introduction

Cytochromes P450 (CYPs, P450s) are enzymes in a monooxygenase superfamily containing a heme-thiolate as a prosthetic group, which are widely found throughout nature from eubacteria and archaeobacteria to humans [1,2]. Despite the differences in the phylogenetic origin, their structural folds and catalytic mechanisms are similar [3,4]. The fold of P450 enzymes appears to be uniquely adapted to the heme-thiolate chemistry required for oxygen activation, binding of a redox partner, and stereochemical requirement of substrate recognition [5].

Actinomycetes produce two-thirds of microbially derived antibiotics used in human and veterinary medicine [6,7]. The soil-dwelling, filamentous Gram-positive bacterium *Streptomyces coelicolor* is the prototypic strain of actinomycetes species. Its genome sequence has facilitated to understanding of the genetic and physiological bases of the large class of actinomycetes [6]. The

chromosome is 8.7 Mb long with a 72% G + C content and is predicted to contain 7825 protein encoding genes [6]. Eighteen P450s, six ferredoxin, and four ferredoxin reductase genes are distributed across the *S. coelicolor* genome, with nine of the P450 genes arranged in polycistronic organization with other genes [8,9].

Structural studies of P450 enzymes from *S. coelicolor* have been focused on the biosynthesis of antibiotics [7]. The crystal structure of *S. coelicolor* CYP154C1 showed a novel open substrate channel going (into the heme), allowing substrate access to the active site [10]. This feature provides the structural basis for the catalytic activity of CYP154C1 toward both 12- and 14-membered rings of macrolide antibiotics [10]. The structure of CYP154A1 showed that its heme orientation is inverted 180° to place the vinyl and propionic acid side chains of the pyrrole rings on the opposite sides of the heme plane from other known P450 enzymes [7,11]. CYP158A2 is located in an operon just downstream from the type III polyketide synthase involved in the biosynthesis of flaviolin. The structure of CYP158A2 bound to flaviolin was determined to have two molecules of flaviolin in the active site, which are arranged in a quasi-planar stacking way to allow oxidative C–C coupling of flaviolin molecules to produce flaviolin dimers [7,12]. CYP170A1 catalyzes the final two steps in the biosynthesis of the antibiotic

* Corresponding authors. Address: Department of Biological Sciences, Konkuk University, 120 Neungdong-ro, Gwangjin-gu, Seoul 143-701, Republic of Korea. Fax: +82 2 3436 5432.

E-mail addresses: lkang@konkuk.ac.kr (L.-W. Kang), donghak@konkuk.ac.kr (D. Kim).

¹ These authors contributed equally to this work.

albaflavenone. The crystal structure of CYP170A1 helped in the discovery of the bifunctional activity of P450. Its structure includes an alpha-helical barrel structure essential for the terpene synthase activity [13].

In this study we cloned, overexpressed, and purified *S. coelicolor* CYP105N1, which is involved in the biosynthesis of bacterial siderophores, and its crystal structure was determined at 2.9 Å resolution. The characterization of the structural and catalytic properties of this protein helps the functional basis of P450 enzymes in utilization of the essential metals.

2. Materials and methods

2.1. Chemicals and enzymes

The coelibactin analog (methyl(4*S*,5*S*)-dihydro-5-methyl-2-phenyl-4-oxazolecarboxylate) was purchased from Sigma Aldrich (St. Louis, MO). Other chemicals were of the highest grade commercially available.

2.2. Construction of expression plasmids

The general approach was as described previously [14,15]. The genomic DNA from *S. coelicolor* was isolated using a DNeasy Blood & Tissue kit (Qiagen, Valencia, CA). The open reading frame for CYP105N1 and an added (His)₆-C-terminal tag were amplified using PCR, with forward and reverse primers (5'-CGAATCATATGACACCCCGAATCC-3', 5'-ATTATTTCTAGACCGGAAGCTTTTGTGATGATGATGATGATGCCAGTCCACCATC-3'), and the amplified PCR fragments were cloned into the pCW(ori⁺) vector using the *Nde*I and *Xba*I restriction sites.

2.3. Enzyme expression and purification

Expression and purification of the CYP105N1 enzyme were carried out as previously described with some modifications [16]. Briefly, the *Escherichia coli* strain DH5α transformed with pCW(ori⁺) vectors was inoculated into LB medium containing ampicillin (100 μg/ml), cultured overnight. One liter of TB medium containing ampicillin (100 μg/ml) was inoculated with the overnight culture (1:100 dilution) and grown at 37 °C. When the culture reached an OD₆₀₀ of 0.6, 1.0 mM IPTG and 0.5 mM δ-aminolevulinic acid were added. The expression cultures were further grown at 28 °C with shaking at 200 rpm for 24 h in Fernbach flasks. Bacterial soluble fractions containing CYP105N1 were prepared from TB expression cultures of *E. coli* DH5α and isolated by ultracentrifugation. CYP105N1 proteins were purified using a Ni²⁺-NTA (Qiagen, Valencia, CA) and Superdex 200 10/300 GL columns (GE healthcare, Pittsburgh, PA), as described previously [17]. After size-exclusion chromatography, the eluted fraction containing P450 enzyme was pooled and dialyzed against 500 volumes of 10 mM Tris-HCl buffer (containing 0.5 M sodium chloride 0.1 mM EDTA) at 4 °C. The dialyzed fraction was further concentrated using Amicon Ultra-15 Centrifugal Filter Units (Millipore, Billerica, MA) for crystallization.

2.4. Spectroscopic characterization

Sodium dithionite was added to reduce the purified ferric CYP105N1 enzymes. The CO-ferrous P450 complexes were generated by passing CO gas through solutions of the ferrous P450. UV-visible spectra were collected on a CARY 100 Varian spectrophotometer in 100 mM potassium phosphate buffer (pH 7.4) at room temperature.

2.5. Spectral binding titrations

Purified CYP105N1 enzyme was diluted to 2 μM in 100 mM potassium phosphate buffer (pH 7.4) and divided between two glass cuvettes. Spectra (350–500 nm) were recorded with subsequent additions of ligands (coelibactin analog or estradiol) using a CARY 100 Varian spectrophotometer [18]. The difference in absorbance between the wavelength maximum and minimum was plotted against substrate concentration [19].

2.6. Protein crystallization, data collection, and structure determination

Crystallization conditions were initially screened using the sitting drop vapor-diffusion method with a Hydra II eDrop automated pipetting system (Matrix) at 287 K. Drops consisted of 0.5 μl protein solution (7 mg ml⁻¹) and 0.5 μl reservoir solution and were equilibrated against 70 μl of reservoir solution at 15 °C. The initial crystallization conditions tested were from the Wizard kit (Emerald BioSystems, Bedford, MA). After day 2, a crystal was observed in Wizard-2 (condition No. 24; 0.1 M imidazole pH 8.0, 0.2 M NaCl, 30% (w/v) PEG 8000). This crystal was optimized using the hanging drop vapor-diffusion method. The optimized crystal was cryoprotected in the reservoir solution supplemented with 20% (v/v) glycerol. The crystal was mounted in a loop and transferred to a cryoprotectant solution prior to cooling in liquid nitrogen.

The crystal was analyzed on beamline BL26B1 (Spring-8, Wako, Saitama, Japan) using a Jupiter210 (Rigaku/MSC) CCD detector. Diffraction data were collected to 2.9 Å resolution and were integrated and scaled using HKL-2000. The crystal belonged to a hexagonal primitive space group (P6₁22), with unit-cell parameters $a = b = 133.1$, $c = 227.1$ Å. Matthews coefficient analysis indicated that there might be two molecules present in the asymmetric unit ($V_m = 3.22$ Å³ Da⁻¹), giving a solvent content of 61.8%. The final statistics of data collection and processing details are summarized in Table 1.

The structure was determined by molecular replacement using CYP105P1 from *S. avermitilis* (PDB ID: 3E5J, sequence identity 42%). The initial phases were calculated using the Phaser program in CCP4 package [20]. The model was further manually built using COOT [21] and refined using REFMAC5. The structural figures were prepared using PyMol (<http://pymol.sourceforge.net/>).

Table 1
Data collection and refinement statistics.

<i>Data collection</i>	
Beamline	Spring-8 BL26B1
Wavelength (Å)	1.0
Resolution range (Å)	50.00–2.80 (2.85–2.80)
Space group	P6 ₁ 22
Unit-cell parameters (Å)	$a = b = 133.0$, $c = 227.1$
Total No. of reflections	280,350
No. of unique reflections	98,528
Completeness (%)	88.8 (55.3)
Molecules per asymmetric unit	2
Solvent content (%)	60.8
Average $I/\sigma(I)$	2.5 (0.9)
R_{sym}^a (%)	19.2 (39.9)
Multiplicity	2.8 (1.6)
<i>Refinement</i>	
Resolution range (Å)	20.0–2.9
R_{work}/R_{free}	28.1/30.2
B value	46.0
R.M.S.D	
Bond	0.026
Angle	3.5
Waters	59

^a $R_{sym} = \sum_h \sum_i |I(h)_i - \langle I(h) \rangle| / \sum_h \sum_i I(h)_i$, where $I(h)$ is the intensity of reflection h , \sum_i is the sum over all reflections, and $\langle I(h) \rangle$ is the sum over i measurements of reflection h . Values in parentheses are for highest-resolution shell.

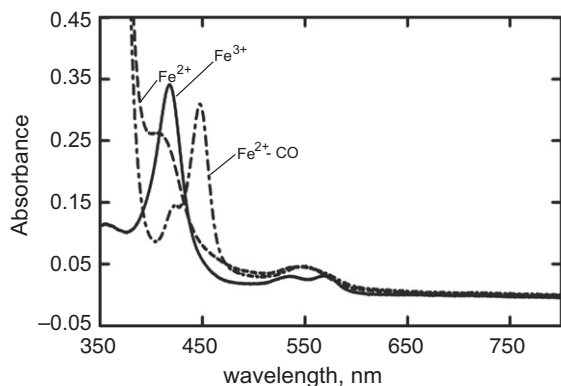


Fig. 1. Spectra of the purified CYP105N1. Absolute spectra of the ferric (—), the ferrous (---), and the ferrous carbon monoxide protein (- · - ·).

2.7. CYP105N1-coelibactin complex model by molecular docking

Docking was performed with the program AutoDock Vina [22]. The determined CYP105N1 structure was taken as a receptor for docking study with a ligand, coelibactin. The coelibactin molecule

was drawn using PRODRG server [23] and used for docking. The docking was performed on the substrate binding pocket of CYP105N1 with the default parameters. For molecular docking, water molecules in the substrate-binding pocket were removed from PDB. The resulting docked models were verified by superimposition with other substrate-bound P450 structures.

2.8. P450 enzyme activity assay

Estradiol hydroxylation by CYP105N1 was determined using an HPLC method. The reaction mixture included 1.0 nmol purified P450 enzyme and 100 mM H_2O_2 in 0.50 ml of 100 mM potassium phosphate buffer (pH 7.4), along with 400 μ M estradiol. Control experiments were performed without support of H_2O_2 or without P450 enzyme. Incubations were generally done for 30 min at 37 °C and were terminated by addition of 1 ml of CH_2Cl_2 . The reaction products were recovered from the organic phase and dried under N_2 . The reaction products were analyzed by HPLC using an ODS (C18) column (4.6 mm \times 150 mm, 3 μ m, Phenomenex, Torrance, CA) at a flow rate of 1.0 ml⁻¹, monitoring A_{280} . The mobile phase was 20% CH_3CN (v/v) in 20 mM $NaClO_4$ (pH 2.5) followed by a linear gradient increasing to 50% CH_3CN (v/v) over 20 min, then holding for 5 min.

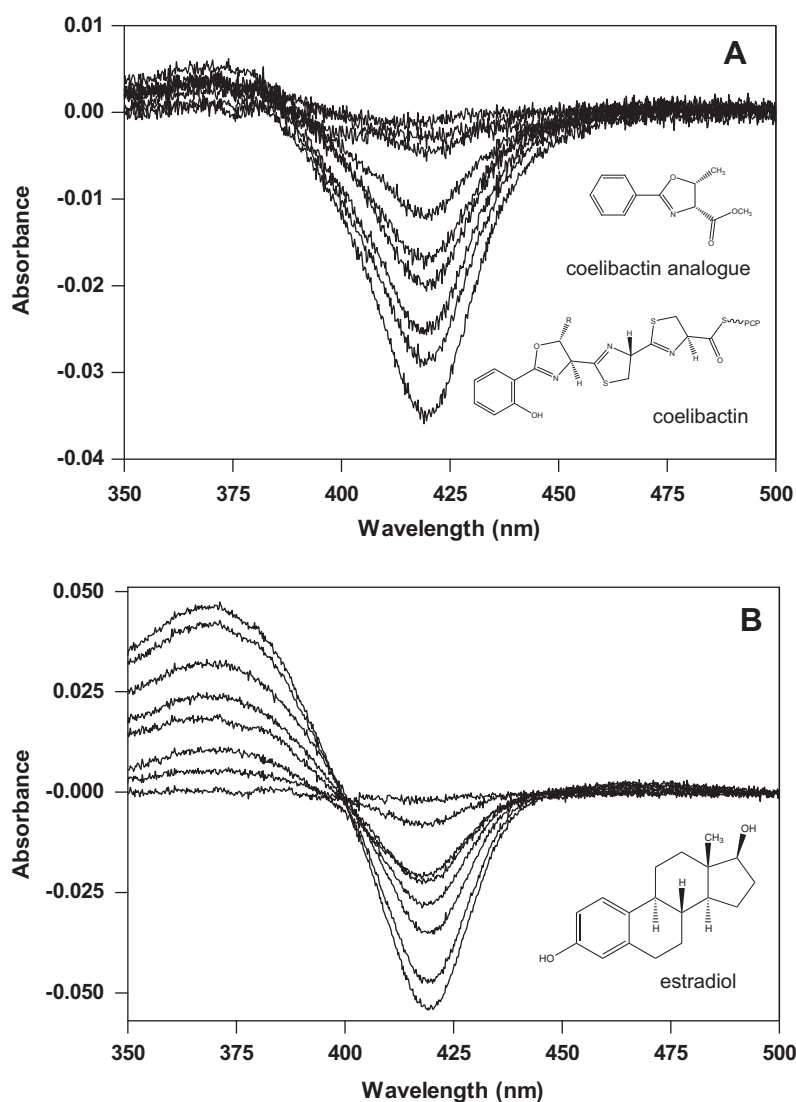


Fig. 2. Titration of CYP105N1 with a coelibactin analog and estradiol. Increasing concentrations (1–50 μ M) of the coelibactin analog (A) and estradiol (B) were added to both the sample and reference cuvettes.

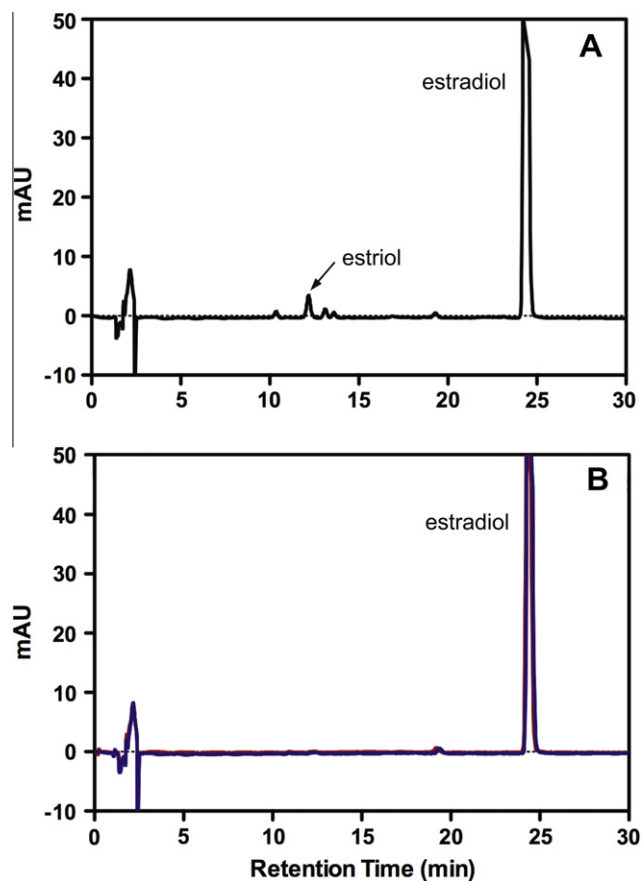


Fig. 3. HPLC of products formed in the reaction of CYP105N1 with estradiol. Estradiol hydroxylation reaction by CYP105N1 was performed using H_2O_2 (A) or without support of H_2O_2 (red, B). Control reaction without CYP105N1 enzyme was performed with support of H_2O_2 (blue, B). (For interpretation of the references to colour in this figure legend, the reader is referred to the web version of this article.)

3. Results

3.1. Expression and purification of CYP105N1

The reduced CO-binding spectrum in the whole cell culture showed an expression level of ~ 350 nmol P450 holoenzyme per liter of culture medium (data not shown). After ultracentrifugation, the expressed P450 protein was found in the soluble fraction and successfully purified using affinity and size exclusion columns. The resulting protein migrated on SDS-PAGE as a major band at 45 kDa, as expected for the open reading frame of the CYP105N1 gene with an added His-tag (data not shown).

3.2. Spectral properties of CYP105N1

The reduced CO binding difference spectrum of purified CYP105N1 had an absorbance maximum at 448 nm (Fig. 1). Examination of the absolute spectrum showed that the ferric form of the protein was in the low spin state, with a Soret band at 418 nm, while the ferrous protein had a broad absorption peak around 420 nm (Fig. 1). The α - and β -bands of the ferric P450 were at 570 and 535 nm, respectively (Fig. 1).

3.3. Binding of coelibactin analogue and estradiol to CYP105N1

Because coelibactin was not available, a truncated coelibactin analog containing a 2-phenyl-4,5-dihydrooxazole moiety (Fig. 2)

and estradiol (E_2) were used as surrogate ligands for CYP105N1 in this study. Titration of purified CYP105N1 with a coelibactin analog and estradiol showed “Type I” spectral changes, with an increase at 390 nm and decrease at 420 nm, giving a low-spin hexacoordinated P450 heme (Fig. 2). The calculated K_d values are 6.7 ± 1.0 μM for the coelibactin analog and 10.7 ± 2.6 μM for estradiol, respectively.

3.4. Catalytic activities of CYP105N1

Oxidation reaction of estradiol (E_2) was analyzed as a surrogate substrate for CYP105N1. Purified CYP105N1, supported by H_2O_2 , oxidized estradiol to yield a product eluting at 12 min in HPLC (Fig. 3). The product was identified as estriol by co-chromatography with authentic estriol. The control reactions without H_2O_2 sup-

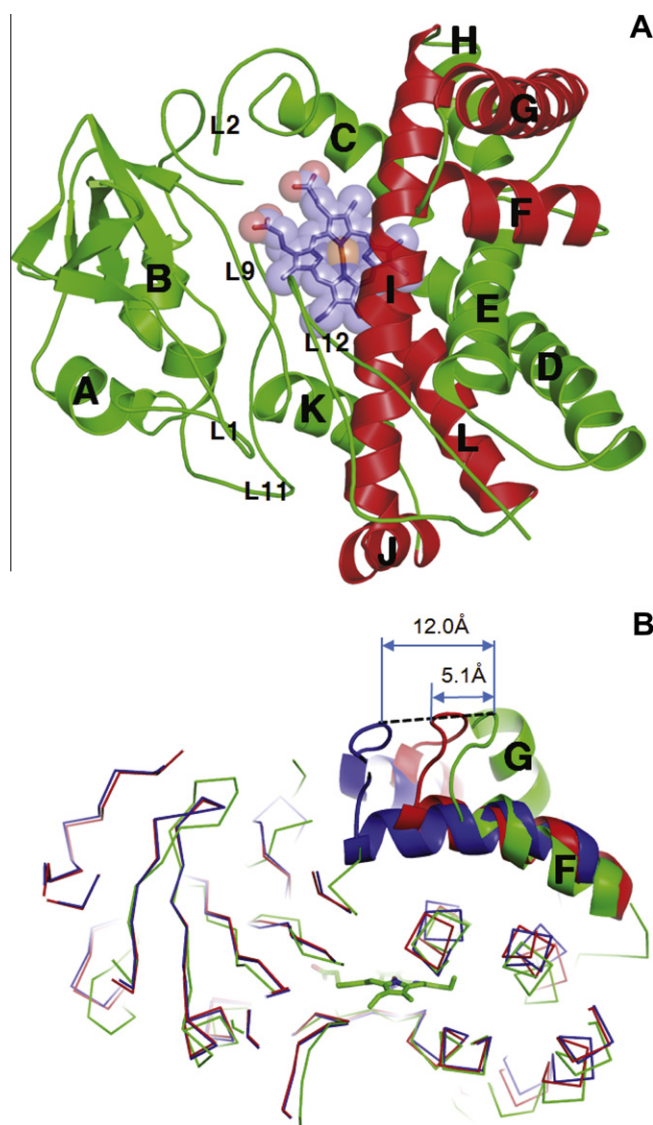


Fig. 4. Overall structure of CYP105N1 and wide open conformation of substrate binding pocket. (A) Overall structure of CYP105N1 and its heme group at the active site. Cartoon representation of CYP105N1 with its heme group. The helices and active site loops of CYP105N1 are labeled as Supplementary Fig. S1. The prosthetic heme group was shown as sticks with spheres. The core helices of P450s are shown in red. (B) Overlap of $\text{C}\alpha$ trace models of CYP105N1 (green), free P450_{cam} (red), and camphor-bound P450_{cam} (blue) are shown. The F and G helices are shown as helices. The distances between the loops connecting F and G helices are shown. (For interpretation of the references to colour in this figure legend, the reader is referred to the web version of this article.)

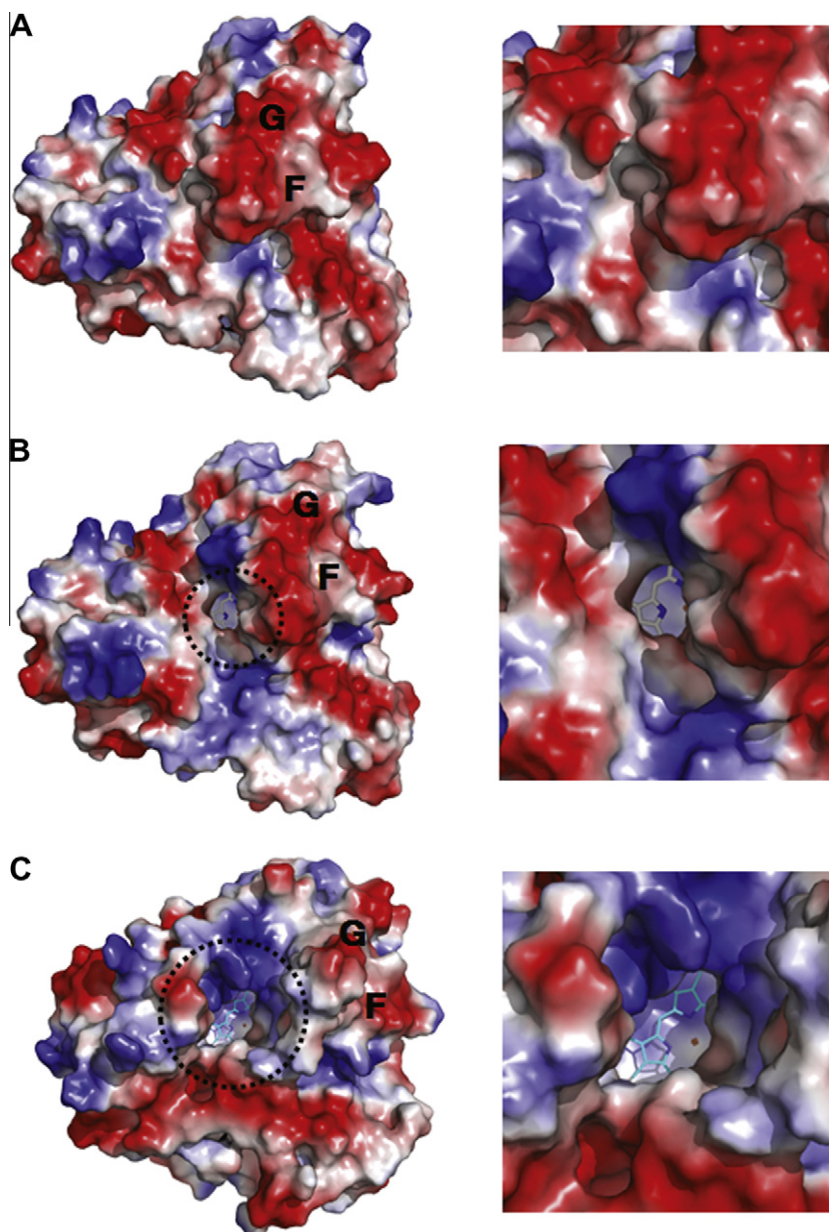


Fig. 5. Electrostatic molecular surface of P450s and their substrate binding channels. Top views of electrostatic molecular surfaces of (A) camphor-bound, (B) substrate-free P450_{cam}, and (C) CYP105N1 are shown with the enlarged views of substrate binding channels. The substrate binding channels of free P450_{cam} and CYP105N1 are marked as dotted circles, in which the prosthetic heme groups are shown as sticks. The positions of the F and G helices are labeled on the surface.

port or without CYP105N1 enzyme did not produce the metabolic product (Fig. 3).

The calculated turnover rate was approximately 0.16 nmol estriol produced/min/nmol P450. However, no product was observed in the attempted reaction with the coelibactin analog (data not shown).

3.5. Overall structure of CYP105N1

CYP105N1 from *S. coelicolor* was crystallized in the hexagonal space group of P6₁22, and two molecules existed in the asymmetric unit. The structure of CYP105N1 was determined by molecular replacement using *S. avermitillis* CYP105P1 (PDB ID: 3E5J) [24] and refined at 2.9 Å resolution (Table 1). Electron-density maps for almost all the residues of CYP105N1 were clearly observed, except the N-terminal 17 residues and a flexible loop of residues 84–87.

CYP105N1 had a generally conserved tertiary fold common in P450s (Supplementary Fig. 1). The iron atom of the prosthetic heme group was coordinated with the conserved Cys360 (2.1 Å).

3.6. Open conformation of CYP105N1 substrate binding pocket

Although the overall folding was well conserved (Fig. 4A), the conformation of the substrate binding pocket was quite different from other P450s. The CYP105N1 substrate binding pocket had a wide open conformation compared to most P450s; e.g., the CYP105N1 F and G helices were shifted outward by 5.1 and 12.0 Å compared to those of camphor-bound and free forms of P450_{cam} (PDB ID: 3L63, 3L62 [25]), respectively (Fig. 4B). In many of microbial P450 structures, the F and G helices had direct interactions with neighbor loops including the B' helix and L12 loop regions, to shape the narrow substrate binding pocket. However, the

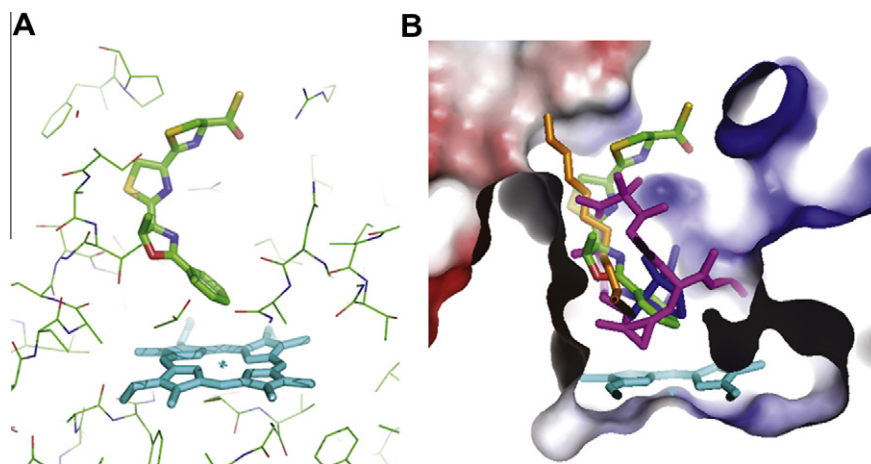


Fig. 6. Superimposed active site structures of substrate-bound P450s. (A) Active site of the coelibactin-docked CYP105N1 model. The heme group is shown in cyan and the docked coelibactin is shown in atom colors of carbon as green; nitrogen, blue; oxygen, red; and sulfur, yellow. (B) Superimposed active sites of camphor (blue)-bound P450_{cam}, epothilone B (pink)-bound P450_{epoK}, fatty acid (orange)-bound P450_{BSB}, and coelibactin-bound CYP105N1. Substrates and heme groups are shown as sticks with electrostatic molecular surface of the CYP105N1 substrate binding channel. (For interpretation of the references to colour in this figure legend, the reader is referred to the web version of this article.)

F and G helices of CYP105N1 did not interact with the neighbor loops and therefore possessed a wide open conformation. The F and G helices in P450_{cam} were bent on I helix, which interacted with the hydrophobic C-terminal loop L12 and B' helix, respectively (Supplementary Fig. 2A). The hydrophobic C-terminal loop L12 in P450_{cam} was inserted deep inside the substrate binding pocket and held together by neighboring secondary structures of the L9, L10, G, and I helices and especially the N-terminal loop L1 and F helix. In CYP105N1, the N-terminal loop L1 was much shorter, and L12 lost the interactions with both L1 and F helix (Figs. 4B and 5). P450_{epoK} has the longer loop between the F and G helices, which had interactions with the L12 and B' helix (Supplementary Fig. 2B). In P450_{epoK}, the F and G helices are only slightly longer than those of CYP105N1. However, the B' helix moved further into the F and G helices and made tight interactions with them (Supplementary Fig. 2C).

As a result, the open CYP105N1 substrate binding pocket was 4299 Å³, which is much bigger than other P450s (e.g., the substrate-bound and unbound substrate binding pockets of P450_{cam} are only 1482 and 2274 Å³ (Fig. 5)[26]). The heme group of CYP105N1 was directly exposed to the solvent through the broad channel of approximately 11 Å width, which could facilitate the binding of a large substrate such as a peptidyl carrier protein-bound substrate (Fig. 5C).

4. Discussion

S. coelicolor has a cluster of genes predicted to synthesize a siderophore-related non-ribosomally encoded peptide designated as coelibactin [27,28]. CYP105N1 is the product of the SCO7686 gene among the cluster, and this cluster also contains the SCO7676 gene for ferredoxin, a putative electron transfer protein for P450 enzyme. Kallifidas et al. [27] discovered a cluster of genes predicted to directly synthesize a siderophore-related non-ribosomally encoded peptide, designated as coelibactin, in a previous study involving *S. coelicolor* mutants lacking the zinc-responsive *Zur* repressor. *Zur* controls the expression of these clustered genes, and disruption of any of these genes suppressed the *Zur* sporulation phenotype, suggesting that deregulation of coelibactin synthesis inhibits sporulation [27]. The SCO7686 gene (for CYP105N1) and the SCO7676 gene (for ferredoxin) are among the *Zur* responsive genes. In addition, an *absC* binding site adjacent to *Zur* binding

site was identified, and dual regulation of coelibactin expression was demonstrated [28]. The regulation of the coelibactin gene cluster by *Zur* and *absC* indicates that coelibactin might have a physiological role for zinc-dependent antibiotic production in *S. coelicolor* [28]. However, it should be noted that coelibactin is still a theoretical substrate for CYP105N1, generated by bioinformatics approaches, and its real chemical structure is not identified yet.

Chun et al. [29] studied the electron transport pathway for *S. coelicolor* P450 enzymes. *S. coelicolor* possesses six ferredoxins (Fdxs)² and four ferredoxin reductases (FDRs) in its genome [9,28]. CYP105D5 from *S. coelicolor* bound fatty acids tightly and produced hydroxylated products when electrons were delivered using *S. coelicolor* FDR1 and Fdx4 [29]. The genes coding for FDR1, Fdx4, and P450 105D5 were found to be located close together in the *S. coelicolor* genome [29]. Neither putidaredoxin reductase (PdR)/putidaredoxin (Pd) from *Pseudomonas putida* nor spinach FDR/Fdx was able to support the catalytic reaction of CYP105N1 (data not shown). The primary electron pathway to CYP105N1 involving *S. coelicolor* Fdxs and FDRs is currently under investigation. In this study, H₂O₂ was used as a surrogate substrate for CYP105N1 but it should be noted that some phenol compounds could be non-enzymatically oxidized by oxygen species.

Coelibactin is a putative substrate of CYP105N1, with an elongated shape composed of three directly-connected five-member rings, a benzene-ring, and a sulfur-carbonyl group attached at each end, respectively. With the failure to obtain a cocrystal structure of CYP105N1 with coelibactin analog, we docked coelibactin to the CYP105N1 structure and verified the docked models by comparing the previous reported cocrystal structures of P450s and their substrates (Fig. 6)[25,30–32]. In a model (among five top-scored models), the coelibactin molecule was superimposed well with the other substrates such as camphor, epothilones, and palmitic acid. The best docked model of CYP105N1-coelibactin showed that coelibactin was bound in the internal active site, and the terminal benzene ring of coelibactin was positioned just above the heme distal surface next to the oxygen binding site (<4 Å away from the iron atom of heme group). Coelibactin was mainly recognized by the three loops L9, L10, and L12 (Fig. 6). Three five-membered rings

² Abbreviations used: Fdxs, ferredoxins; PdR, putidaredoxin reductase Pd, putidaredoxin.

of coelibactin showed a similar bent shape bound structure with palmitic acid in P450_{BSβ} [33]; it interacted with the substrate-binding pocket mostly via hydrophobic interactions (Fig. 6). The terminal sulfur-carbonyl group had bi-furcated hydrogen bond interactions with the guanidine group of Arg95. The wide open conformation of the CYP105N1 substrate binding pocket helps substrates with larger volumes bind more easily. The loop structure of the B'-helix region in CYP105N1 residues 84–95 also makes the substrate binding pocket easily accessible and flexible.

In this study, we overexpressed and purified CYP105N1 from *S. coelicolor* and performed biochemical and structural characterization. CYP105N1 has the structure of a wide open binding pocket with well conserved P450 folding. It catalyzed the hydroxylation of estradiol to produce estriol. The structure–function studies of *S. coelicolor* CYP105N1 enzyme reported here help understand functional roles of P450 enzymes in the biosynthetic pathway for the siderophore-related compounds in actinomycetes species.

5. Note

While the current study was under review, Zhao et al. published a report describing a similar structural conformation of CYP105N1 [34]. Their structure also showed a wide-open conformation exposing the heme pocket and long I helix to the solvent.

6. Accession number

Coordinates and structure factors of CYP105N1 have been deposited in the Protein Data Bank (Accession No. 4FXB).

Acknowledgments

This work was supported by National Research Foundation of Korea (NRF) Grant funded by the Korea government (MEST) (No. 2011-0016509). We thank F. Peter Guengerich for a critical review of the manuscript.

Appendix A. Supplementary data

Supplementary data associated with this article can be found, in the online version, at <http://dx.doi.org/10.1016/j.abb.2012.09.001>.

References

- [1] P.R. Ortiz de Montellano, J.J. De Voss, in: P.R. Ortiz de Montellano (Ed.), *Cytochrome P450: Structure, Mechanism, and Biochemistry*, Plenum Press, New York, 2005, pp. 183–245.
- [2] F.P. Guengerich, *Nat. Rev. Drug Discov.* 1 (2002) 359–366.
- [3] Z. Zhang, O. Sibbesen, R.A. Johnson, P.R. Ortiz de Montellano, *Bioorg. Med. Chem.* 6 (1998) 1501–1508.
- [4] C.A. Hasemann, R.G. Kurumbail, S.S. Boddupalli, J.A. Peterson, J. Deisenhofer, *Structure* 3 (1995) 41–62.
- [5] T.L. Poulos, E.F. Johnson, in: P.R. Ortiz de Montellano (Ed.), *Cytochrome P450: Structure, Mechanism, and Biochemistry*, Plenum Press, New York, 2005, pp. 87–114.
- [6] S.D. Bentley, K.F. Chater, A.M. Cerdeno-Tarraga, G.L. Challis, N.R. Thomson, K.D. James, D.E. Harris, M.A. Quail, H. Kieser, D. Harper, A. Bateman, S. Brown, G. Chandra, C.W. Chen, M. Collins, A. Cronin, A. Fraser, A. Goble, J. Hidalgo, T. Hornsby, S. Howarth, C.H. Huang, T. Kieser, L. Larke, L. Murphy, K. Oliver, S. O'Neil, E. Rabinowitsch, M.A. Rajandream, K. Rutherford, S. Rutter, K. Seeger, D. Saunders, S. Sharp, R. Squares, S. Squares, K. Taylor, T. Warren, A. Wietzorrek, J. Woodward, B.G. Barrell, J. Parkhill, D.A. Hopwood, *Nature* 417 (2002) 141–147.
- [7] D.C. Lamb, F.P. Guengerich, S.L. Kelly, M.R. Waterman, *Expert Opin. Drug Metab. Toxicol.* 2 (2006) 27–40.
- [8] D.C. Lamb, L. Lei, B. Zhao, H. Yuan, C.J. Jackson, A.G. Warrilow, T. Skaug, P.J. Dyson, E.S. Dawson, S.L. Kelly, D.L. Hachey, M.R. Waterman, *Appl. Environ. Microbiol.* 76 (2010) 1975–1980.
- [9] D.C. Lamb, T. Skaug, H.L. Song, C.J. Jackson, L.M. Podust, M.R. Waterman, D.B. Kell, D.E. Kelly, S.L. Kelly, *J. Biol. Chem.* 277 (2002) 24000–24005.
- [10] L.M. Podust, Y. Kim, M. Arase, B.A. Neely, B.J. Beck, H. Bach, D.H. Sherman, D.C. Lamb, S.L. Kelly, M.R. Waterman, *J. Biol. Chem.* 278 (2003) 12214–12221.
- [11] L.M. Podust, H. Bach, Y. Kim, D.C. Lamb, M. Arase, D.H. Sherman, S.L. Kelly, M.R. Waterman, *Protein Sci.* 13 (2004) 255–268.
- [12] B. Zhao, F.P. Guengerich, M. Voehler, A. Bellamine, D.C. Lamb, M. Izumikawa, L. Lei, L.M. Podust, M. Sundaramoorthy, J.A. Kalaitzis, L.M. Reddy, S.L. Kelly, B.S. Moore, D. Stec, M. Voehler, J.R. Falck, T. Shimada, M.R. Waterman, *J. Biol. Chem.* 280 (2005) 11599–11607.
- [13] B. Zhao, L. Lei, D.G. Vassilyev, X. Lin, D.E. Cane, S.L. Kelly, H. Yuan, D.C. Lamb, M.R. Waterman, *J. Biol. Chem.* 284 (2009) 36711–36719.
- [14] D. Kim, F.P. Guengerich, *Biochemistry* 43 (2004) 981–988.
- [15] D. Kim, E.T. Yuki, P. Moenne-Loccoz, P.R. Ortiz de Montellano, *Biochemistry* 45 (2006) 14772–14780.
- [16] D. Kim, M.J. Cryle, J.J. De Voss, P.R. Ortiz de Montellano, *Arch. Biochem. Biophys.* 464 (2007) 213–220.
- [17] D. Kim, Y.S. Heo, P.R. Ortiz de Montellano, *Arch. Biochem. Biophys.* 474 (2008) 150–156.
- [18] C.H. Yun, K.H. Kim, M.W. Calcutt, F.P. Guengerich, *J. Biol. Chem.* 280 (2005) 12279–12291.
- [19] J.B. Schenkman, H. Remmer, R.W. Estabrook, *Mol. Pharmacol.* 3 (1967) 113–123.
- [20] Collaborative Computational Project, *Acta Crystallogr. D Biol. Crystallogr.* 50 (1994) 760–763.
- [21] P. Emsley, K. Cowtan, *Acta Crystallogr. D Biol. Crystallogr.* 60 (2004) 2126–2132.
- [22] O. Trott, A.J. Olson, *J. Comput. Chem.* 31 (2010) 455–461.
- [23] A.W. Schuttelkopf, D.M. van Aalten, *Acta Crystallogr. D Biol. Crystallogr.* 60 (2004) 1355–1363.
- [24] L.H. Xu, S. Fushinobu, H. Ikeda, T. Wakagi, H. Shoun, *J. Bacteriol.* 191 (2009) 1211–1219.
- [25] Y.T. Lee, R.F. Wilson, I. Rupniewski, D.B. Goodin, *Biochemistry* 49 (2010) 3412–3419.
- [26] J. Dundas, Z. Ouyang, J. Tseng, A. Binkowski, Y. Turpaz, J. Liang, *Nucleic Acids Res.* 34 (2006) W116–118.
- [27] D. Kallifidas, B. Pascoe, G.A. Owen, C.M. Strain-Damerell, H.J. Hong, M.S. Paget, *J. Bacteriol.* 192 (2010) 608–611.
- [28] A. Hesketh, H. Kock, S. Mootien, M. Bibb, *Mol. Microbiol.* 74 (2009) 1427–1444.
- [29] Y.J. Chun, T. Shimada, R. Sanchez-Ponce, M.V. Martin, L. Lei, B. Zhao, S.L. Kelly, M.R. Waterman, D.C. Lamb, F.P. Guengerich, *J. Biol. Chem.* 282 (2007) 17486–17500.
- [30] S. Nagano, H. Li, H. Shimizu, C. Nishida, H. Ogura, P.R. Ortiz de Montellano, T.L. Poulos, *J. Biol. Chem.* 278 (2003) 44886–44893.
- [31] T.L. Poulos, B.C. Finzel, I.C. Gunsalus, G.C. Wagner, J. Kraut, *J. Biol. Chem.* 260 (1985) 16122–16130.
- [32] I. Schlichting, J. Berendzen, K. Chu, A.M. Stock, S.A. Maves, D.E. Benson, R.M. Sweet, D. Ringe, G.A. Petsko, S.G. Sligar, *Science* 287 (2000) 1615–1622.
- [33] D.S. Lee, A. Yamada, H. Sugimoto, I. Matsunaga, H. Ogura, K. Ichihara, S. Adachi, S.Y. Park, Y. Shiro, *J. Biol. Chem.* 278 (2003) 9761–9767.
- [34] B. Zhao, S.C. Moody, R.C. Hider, L. Lei, S.L. Kelly, M.R. Waterman, D.C. Lamb, *Int. J. Mol. Sci.* 13 (2012) 8500–8513.